BBA - Molecular Basis of Disease 1865 (2019) 1410–1420

Contents lists available at ScienceDirect

BBA - Molecular Basis of Disease

journal homepage: www.elsevier.com/locate/bbadis

Sequence- and seed-structure-dependent polymorphic fibrils of alpha-synuclein

Goki Tanaka[a], Tomoyuki Yamanaka[a,*], Yoshiaki Furukawa[b], Naoko Kajimura[c], Kaoru Mitsuoka[c], Nobuyuki Nukina[a,*]

[a] Laboratory of Structural Neuropathology, Doshisha University Graduate School of Brain Science, 1-3 Miyakodanitatara, Kyotanabe-shi, Kyoto 610-0394, Japan
[b] Laboratory for Mechanistic Chemistry of Biomolecules, Department of Chemistry, Keio University, 3-14-1 Hiyoshi, Kohoku, Yokohama 223-8522, Japan
[c] Research Center for Ultra-High Voltage Electron Microscopy, Osaka University, 7-1, Mihogaoka, Ibaraki, Osaka 567-0047, Japan

ARTICLE INFO

Keywords:
Alpha-synuclein
Protein aggregation
Parkinson's disease
Amyloid fibrils
Interspecies difference

ABSTRACT

Synucleinopathies comprise a diverse group of neurodegenerative diseases including Parkinson's disease (PD), dementia with Lewy bodies, and multiple system atrophy. These share a common pathological feature, the deposition of alpha-synuclein (a-syn) in neurons or oligodendroglia. A-syn is highly conserved in vertebrates, but the primary sequence of mouse a-syn differs from that of human at seven positions. However, structural differences of their aggregates remain to be fully characterized. In this study, we found that human and mouse a-syn aggregated *in vitro* formed morphologically distinct amyloid fibrils exhibiting twisted and straight structures, respectively. Furthermore, we identified different protease-resistant core regions, long and short, in human and mouse a-syn aggregates. Interestingly, among the seven unconserved amino acids, only A53T substitution, one of the familial PD mutations, was responsible for structural conversion to the straight-type. Finally, we checked whether the structural differences are transmissible by seeding and found that human a-syn seeded with A53T aggregates formed straight-type fibrils with short protease-resistant cores. These results suggest that a-syn aggregates form sequence-dependent polymorphic fibrils upon spontaneous aggregation but become seed structure-dependent upon seeding.

1. Introduction

Neurodegenerative diseases such as Alzheimer's disease, Parkinson's disease (PD), Huntington disease, amyotrophic lateral sclerosis, and prion diseases are recognized to have common molecular pathologies including protein aggregation and inclusion body formation [1]. Lewy bodies (LB) and Lewy neurites, the pathological hallmarks of PD and dementia with Lewy bodies (DLB), contain filamentous forms of alpha-synucleins (a-syn) in neurons, while other neurodegenerative disorders including multiple system atrophy (MSA) also display a-syn deposits in oligodendroglia called glial cytoplasmic inclusions (GCI) [2–4]. These three diseases are collectively called as synucleinopathies [2].

Recent studies demonstrate that MSA is unequivocally caused by a-syn aggregates, in which misfolded proteins undergo self-propagation and are capable of transmitting disease pathology to transgenic mice or to cultured cells [5–8], while as for PD, PD with dementia, and DLB, transmission studies have been unsuccessful [6,7]. Another recent report clearly shows that pathological a-syn in GCIs and LB is conformationally and biologically distinct [9]. These recent reports suggest that distinct conformations of misfolded a-syn strains may be responsible for these diseases. In addition, distinct a-syn strains generated *in vitro* display differential seeding capacities, inducing strain-specific pathology and neurotoxic phenotypes in rodent [10–12]. Namely, it seemed that the conformational differences between distinct a-syn strains are highly related with the disease polymorphisms of synucleinopathies. However, the conformation of polymorphic a-syn fibrils are not directly connected with the neurotoxicity and pathogenicity in rodents, because the amino acid composition of rodent a-syn differs from that of human a-syn, which yielded ambiguous results regarding the conformation of human a-syn fibril.

The mouse a-syn contains substitutions at positions 53, 87, 100, 103, 107, 121, and 122 with human a-syn. *In vivo* assessment of seeding with a-syn aggregates derived from human diseases into mouse brains is relevant for the species barriers as reported in prion disease [13–15].

Abbreviations: AD, Alzheimer disease; PD, Parkinson's disease; DLB, dementia with Lewy bodies; MSA, multiple system atrophy; a-syn, alpha-synuclein; WT, wild type; CBB, Coomassie Brilliant Blue; PFF, pre-formed fibrils; EM, electron microscopy

* Corresponding authors.
E-mail addresses: toyamana@mail.doshisha.ac.jp (T. Yamanaka), nnukina@mail.doshisha.ac.jp (N. Nukina).

https://doi.org/10.1016/j.bbadis.2019.02.013
Received 5 October 2018; Received in revised form 8 January 2019; Accepted 14 February 2019
Available online 18 February 2019
0925-4439/

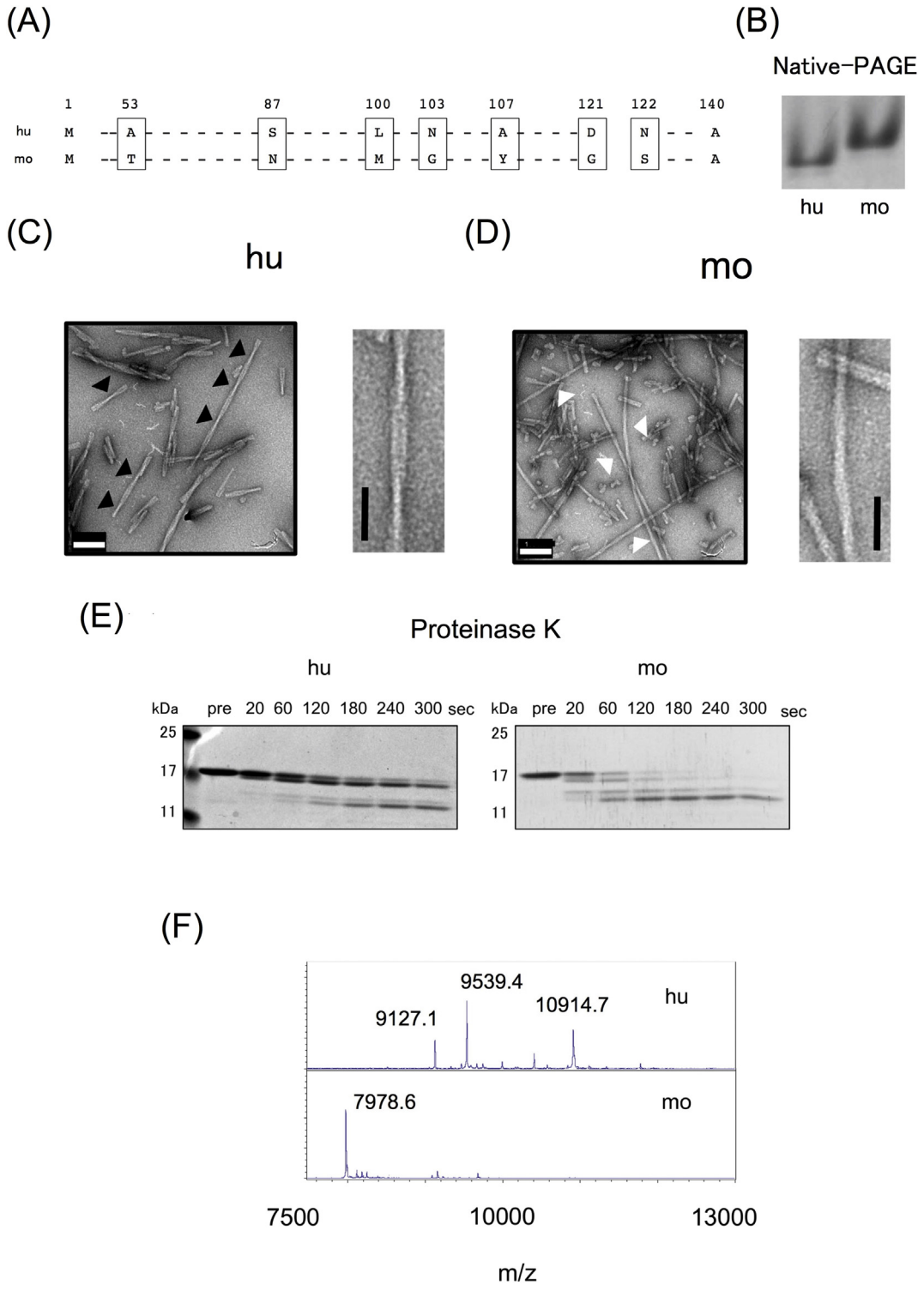

Fig. 1. Biochemical differences in monomeric and aggregation states between human and mouse alpha-synuclein.
Sequence comparison for human (hu) and mouse (mo) a-syn highlighting amino acid differences. (B) Native-PAGE data of human and mouse a-syn. The gel was stained with CBB. (C, D) Electron micrographs of human and mouse a-syn aggregates. Black and white arrowheads indicate twisted sites (C) and straight fibrils (D), respectively. Representative fibrils are shown in right side of each electron micrograph. Human a-syn forms twisted fibrils (twisted) that have wide and narrow segments (C) while mouse a-syn forms straight type fibrils (straight), which does not have clear periodicity (D). Black and white scale bars show 50 nm and 100 nm, respectively. (E) The results of protease partial digestions with proteinase K. "pre" indicates pre-digested samples. Each number indicates reaction times at seconds. (F) MALDI-TOF MS spectra (*m/z* 7500–13,000) of core peptides derived from human and mouse a-syn aggregates. Observed mass is shown in each spectrum. Human and mouse a-syn aggregates are formed by long core (m/z 9127.1, m/z 9539.4, m/z 10,914.7) and short core (m/z 7978.6), respectively. Human and mouse a-syn are designated as hu and mo, respectively.

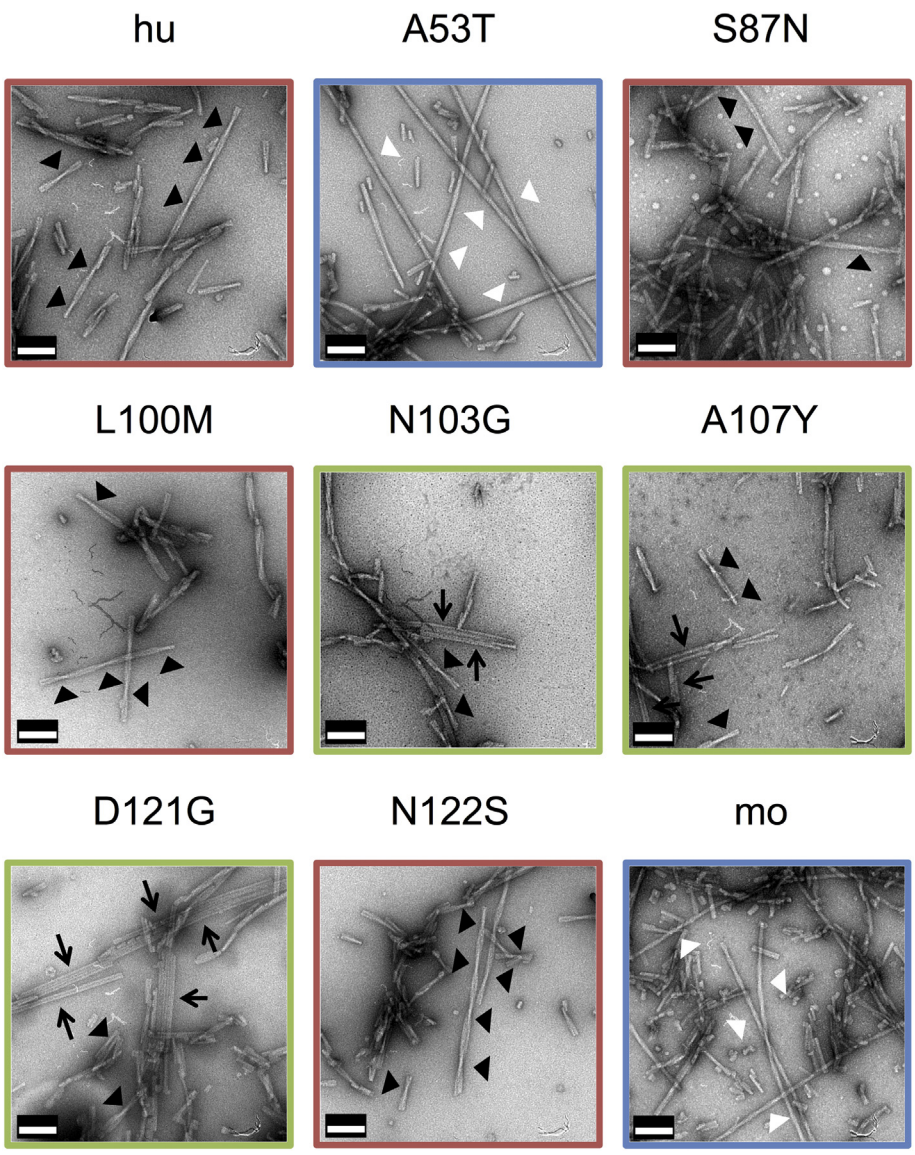

Fig. 2. Alpha-synuclein mutants with single substitution form distinct amyloid fibrils.
Electron micrographs of human WT a-syn, mouse a-syn, and other mutants a-syn. Scale bars show 100 nm. Black and white arrowheads indicate twisted sites and straight filaments, respectively. Black arrows indicate bundle types of filaments. Amyloid fibrils morphologies of mutants were divided into 3 groups: Group A; twisted (red), Group B; straight (blue); Group C; twisted fibrils with bundled ones (green).

The cross-species seeding of human a-syn aggregates attenuate propagation and spreading of aggregates in mouse brain [16–18]. Using chimeric a-syn fibrils, it was reported that interspecies substitutions of human WT a-syn with the mouse a-syn at residues A53 to T and S87 to A (designated as Hu^{TN}) resulted in a higher seeding efficiency than human WT a-syn seeds in both cultures and *in vivo* [19]. These previous researches suggested that human and mouse a-syn are biologically distinct. Cell-free *in vitro* analyses of human and mouse a-syn further demonstrated that these two a-syn fibrils are conformationally distinct, which are also regulated by the two substitutions of A53T and S87N sequences [19–22]. Based on these previous findings, we can speculate that human and mouse a-syn are conformationally and biologically distinct. Thus, the investigation of the difference between human and mouse a-syn is important to uncover the pathogenic contributions to synucleinopathies by a-syn fibril structures. However, studies on the difference between human and mouse a-syn fibrils are quite limited.

In this study, we focused on the structural differences between human and mouse a-syn fibrils to gain new insight into the relationship between pathogenicity of synucleinopathies and a-syn fibril polymorphisms. Using electron microscopy (EM) and protease-resistant core analyses with mass spectrometry, we identified newly polymorphic features of human and mouse a-syn fibrils, which are regulated by an interspecies single substitution, A53T. Furthermore, seeding experiments using those mutants revealed seed-induced structural amplification, suggesting that although the structure of spontaneous aggregates depends on their sequence, the seeds change this spontaneous tendency. Particularly, the structural transmissions of A53T's properties to human WT a-syn by seeding reactions implied that the presence of intracellular pre-formed seeds could induce the conversion of non-pathogenic form into the disease-type-specific pathogenic form *in vivo*.

2. Material and methods

2.1. Preparation of recombinant a-syn

Plasmids pET 15b encoding His-human a-syn and His-mouse a-syn were described previously [18]. Introduction of mutations was performed through Inverse PCR using KOD neo DNA polymerase

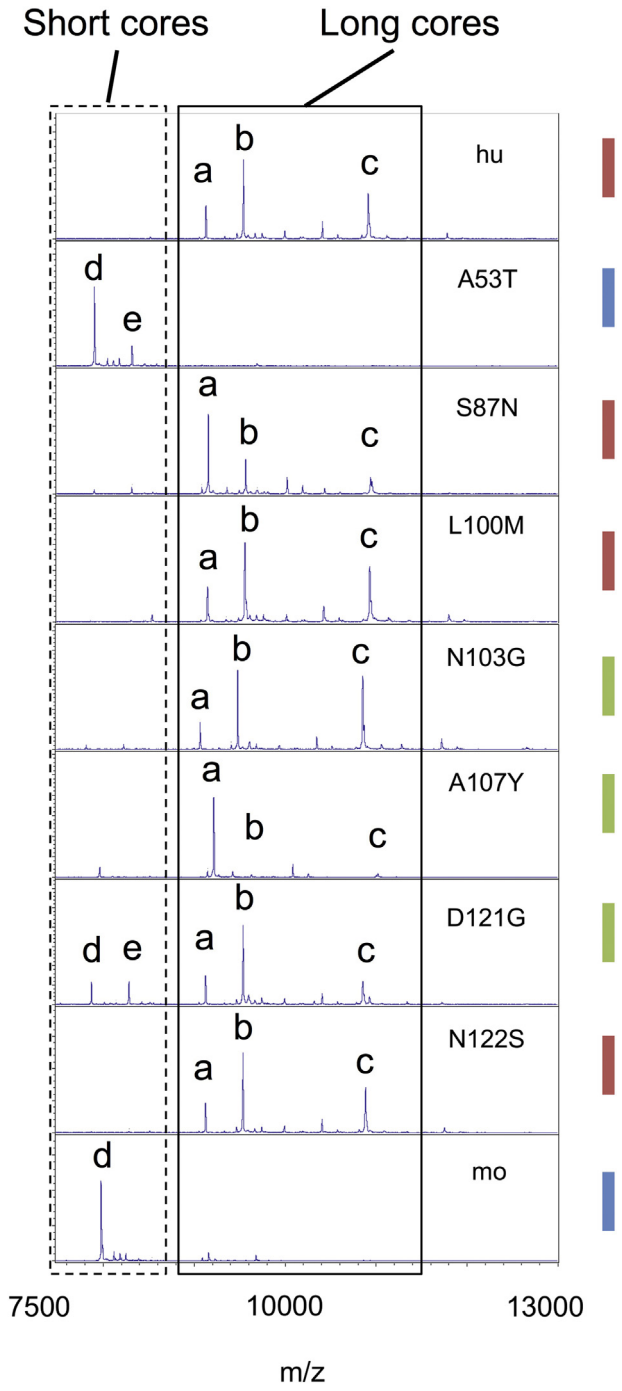

Fig. 3. Alpha-synuclein mutants with single substitution form distinct proteinase K-resistant core revealed by MALDI-TOF MS analysis.
MALDI-TOF MS spectra (m/z 7500–13,000) of core peptides derived from human, mouse, and mutant a-syn aggregates are shown. Segments enclosed in rectangles with a solid and dashed lines are shown for long cores (human-specific spectra area; a, b, c) and short cores (mouse-specific spectra area; d, e), respectively. The classification of morphologies; Group A (red), Group B (blue), and Group C (green) are indicated on the right side.

(TOYOBO) and confirmed by DNA sequencing. Used primers are listed in supplementary table 1. All mutants were established on the site directed mutant of codon 136 (TAC to TAT), which avoids misincorporation of Cys at this position [23]. The *Escherichia coli* (*E. coli*) strain BL21 (DE3) was transformed with the expression vector pET15b encoding a-syn and cultured at 37 °C for several hours and 0.5 M isopropyl 1-thio-β-D-galactopyranoside was added and cultured further for 6 h. To extract proteins from E coli, the cells were lysed with phosphate-buffered saline containing 2% TritonX-100. After sonication and centrifugation, the supernatant was immediately poured into a 15 mL centrifuge tube containing Ni-sepharose beads (GE Healthcare), then rotated for 1 h at 4 °C. The beads were washed twice with 50 mM Tris, 100 mM NaCl, 30 mM imidazole, pH 8.0, and a-syn was eluted with 50 mM Tris, 100 mM NaCl, 250 mM imidazole, pH 8.0. The eluted samples were filtrated with 0.22 μm filter (Millex) to obtain pure protein, and concentrated by Vivaspin Turbo15 (Sartorius). The His-tag was cleaved by Thrombin agarose (Sigma) at 25 °C for 20 h. To eliminate Thrombin agarose, the solution was centrifuged at 15,000 rpm for 3 min, then the supernatant was filtrated with a 0.22 μm filter. After the His tag is removed proteolytically, the obtained a-syn lacks a N-terminal methionine and retains N-terminal Gly-Ser residues that is part of the thrombin recognition site. A-syn protein concentration was determined from the absorption at 280 nm in the presence of 6 M guanidine hydrochloride by using 5690 M^{-1} cm^{-1} or 7450 M^{-1} cm^{-1} as an extinction coefficient. The samples obtained were used for making aggregates.

2.2. In vitro aggregation

Purified a-syn monomers (100 μM) in 150 μL of buffer A (50 mM Tris-HCl, 100 mM NaCl) (pH 8.0) with plastic beads SAN14246 (Sanplatec), were incubated at 37 °C in a shaking incubator Cute Mixer CM-1000 (Tokyo Rikakikai) at 1000 rpm for 7 days. Kinetics of a-syn aggregation was detected by Thioflavin-T fluorescence using Envision at sequential time points (0, 4, 8, 24, 48, 168–192 h). Aggregates were pelleted by spinning at 50,000 rpm for 20 min, resuspended in buffer A (150 μL) and then sonicated using Bioruptor (Biorad). Those aggregates were used for experiments as pre-formed fibrils (PFF). When a seeding reaction was performed, 7.5 μL (5%) of PFF were added to monomeric forms of a-syn (100 μM) in 142.5 μL of buffer A and were incubated. Seeding efficiencies were assessed by Thioflavin T fluorescence at sequential time points (0, 2, 4, 6, 8, 24, 168–192 h). The obtained seed-induced aggregates were used for experiments. Each aggregation experiment was performed for each sample and repeated at least twice.

2.3. Gel electrophoresis

To evaluate the monomeric state of a-syn, we performed Native-PAGE. For Native-PAGE, 2.5 μL of purified a-syn at 100 μM were mixed with 17.5 μL of sample buffer (100 mM Tris-HCl pH 6.8, 20% glycerol, and 0.01% bromophenol blue). Electrophoresis was performed in 12 or 15% (w/v) non-denaturing polyacrylamide gels (excluding SDS) at 20–30 mA for 30 min to 60 min at room temperature with running buffer (100 mM Tris, 100 mM glycine).

For SDS-PAGE, samples were mixed with SDS-containing Laemmli buffer (100 mM Tris-HCl, pH 6.8, 4% SDS, 2% 2-mercaptoethanol, 20% glycerol, and 0.01% bromophenol blue). Electrophoresis was performed in 12 or 15% (w/v) SDS containing polyacrylamide gels (6.25% stacking gel) at 20 mA for 60 min to 120 min at room temperature with running buffer (100 mM Tris, 100 mM glycine, and 0.1% SDS). For both PAGE, samples (10–15 μL) with or without boiling were loaded into the gel. The gels were stained with Coomassie Brilliant Blue (CBB).

2.4. Electron microscopic analysis

Morphological observations of a-syn fibrils were done using an electron microscope H-7000 (Hitachi) at an accelerating voltage of 100 kV. The samples were adsorbed on 400-mesh grids coated by a glow-charged supporting amorphous carbon film and negatively stained with 2% uranyl acetate. The images were recorded on the Orius CCD camera (Gatan) and the width of a fibrillar structure was measured using ImageJ. The means of the number of fibrils were counted from electron micrographs of three different field of view of each sample.

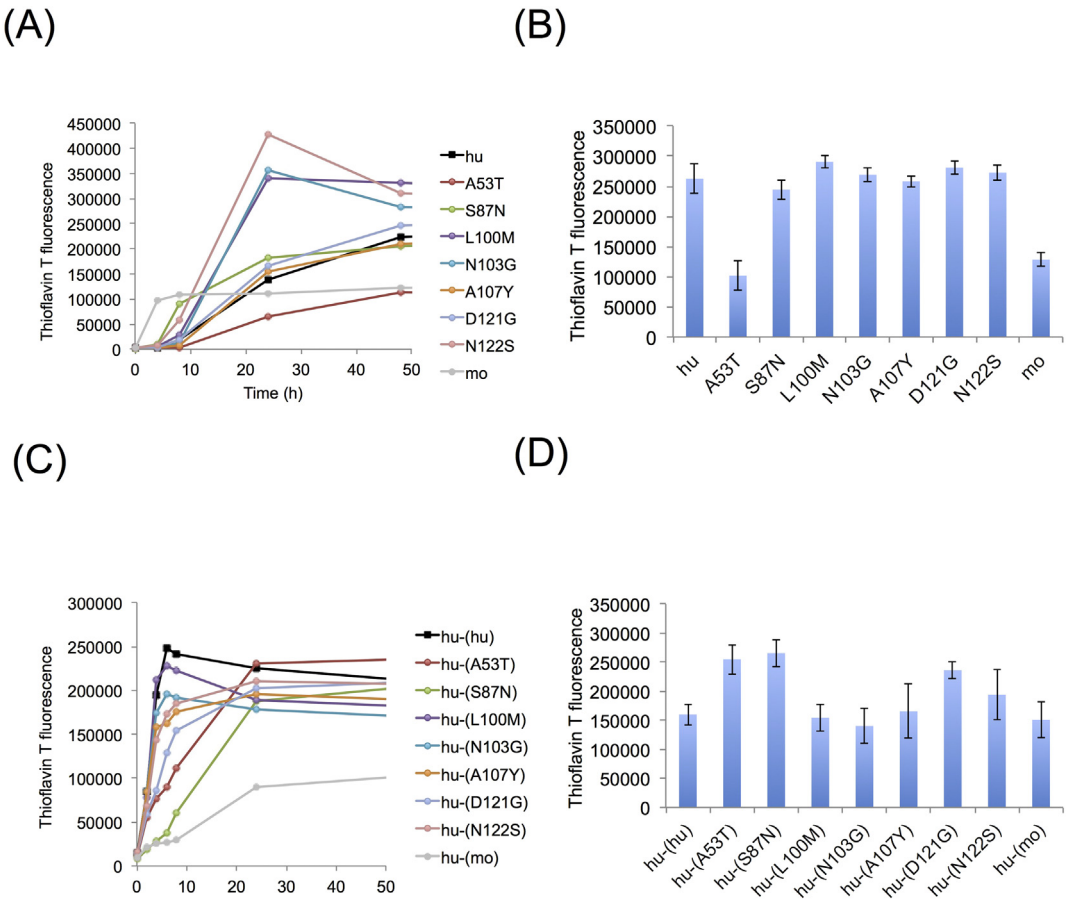

Fig. 4. Aggregation and seeding process were monitored by Thioflavin T fluorescence in human, mouse, and mutant alpha-synuclein.
(A) Kinetics of a-syn aggregation was analyzed by ThT fluorescence at sequential time points (0, 4, 8, 24, 48, and 168 or 192 h). (B) The values of ThT fluorescence in human, mouse, and mutant a-syn incubated at day 7–8 were shown. (C) Seeding efficiencies were assessed by ThT fluorescence at sequential time points (0, 2, 4, 6, 8, 24, and 168 or 192 h). (D) The values of ThT fluorescence in seed-induced aggregation of human WT a-syn incubated at day 7–8 were shown. These experiments were repeated twice. These ThT kinetics data represent averages from the values of two tubes from one experiment.

2.5. Thioflavin T fluorescence

In a 96-well plate, 2.5 μL of a-syn aggregates were mixed with 25 μM ThT in 100 μL of buffer A, and fluorescence was measured in a plate reader (Perkin Elmer) with an excitation filter (430–442 nm cutoff) and an emission filter (485 nm cutoff).

2.6. Protease partial digestion of aggregates

Partial digestion by proteases were performed based on a previous study [24]. A-syn aggregates in buffer A were treated with 4 μg/mL proteinase K (Nacalai) or 40 μg/mL trypsin (Promega). Aliquots were transferred into tubes at different time intervals (20, 60, 120, 180, 240, and 300 s) and treated with the sample buffer for 10 min at 90 °C (proteinase K) or quick stored at −80 °C (trypsin) to immediately arrest further cleavage reaction. The samples were processed to SDS-PAGE to monitor the time course of a-syn cleavage.

2.7. Mass spectral analysis of amyloid cores

A-syn aggregates were treated with proteinase K (4 μg/mL) or lysyl endopeptidase (Wako) for 120 min for amyloid core analysis at 37 °C [25]. Protease-resistant amyloid fibrils were collected by ultracentrifugation (50,000 rpm for 20 min), and the pellets were dissolved in a buffer containing 6 M guanidine hydrochloride and 10 mM Tris·HCl (pH 8.0). The dissociated amyloid fibril peptides were desalted by self-made C18 (3 M Empore solid phase extraction disk) Stage Tip and analyzed by MALDI-TOF MS (autoflex speed TOF/TOF, Bruker Daltonics). Each protease core analysis was performed at least twice.

2.8. Statistical analysis

For comparison between two sample groups, data were first analyzed by *t*-test. We considered the difference between comparisons to be significant when $P < .05$.

3. Results

3.1. Morphological and biochemical differences between human and mouse a-syn aggregates

The substitutions between human and mouse a-syn are distributed unevenly along the sequence; one (A53T) in the N-terminal region, one (S87N) in the NAC region and five (L100M, N103G, A107Y, D121G and N122S) in the C terminal region (Fig. 1A) [20]. Human and mouse a-syn proteins were analyzed by Native-PAGE in order to examine the state of a-syn after purification from *E. coli*. CBB-staining identified strong single band by SDS-PAGE (Fig. S1B), but a mobility difference between human and mouse a-syn was observed in Native-PAGE (Fig. 1B), probably reflecting the charge differences between these proteins.

To test whether these amino acid differences alter the structural properties of aggregates, we compared morphologies of human and mouse a-syn aggregates by EM observation and found their distinct

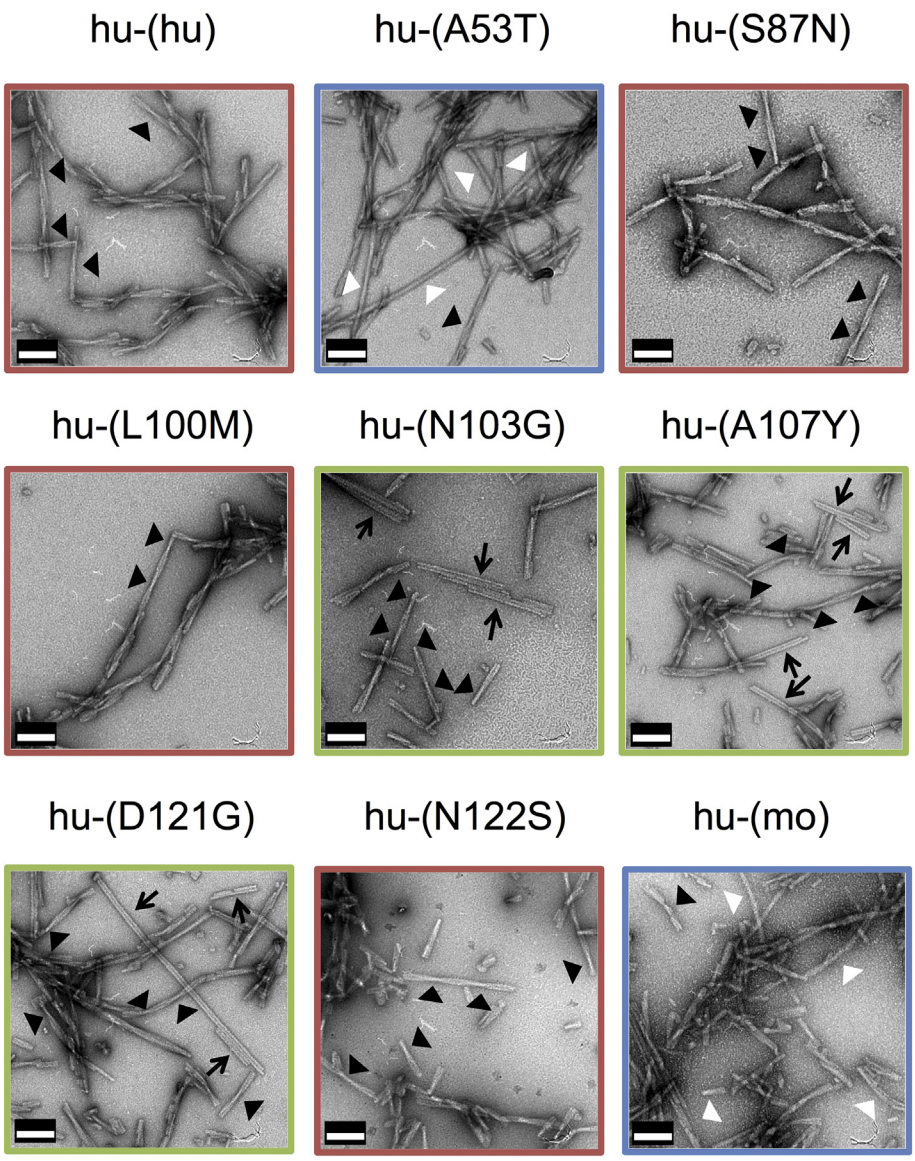

Fig. 5. Morphologies of mutation-dependent structures could be transmitted to human wild-type alpha-synuclein by seeding reactions.
Electron micrographs of aggregates formed from human WT a-syn seeded with human, mouse or other mutants fibrils. Scale bars show 100 nm. Black and white arrowheads indicate twisted sites and straight filaments, respectively. Black arrows indicate bundle types of filaments. Amyloid fibrils morphologies of human WT a-syn aggregates formed by seeding were divided into 3 groups: Group A; twisted (red), Group B; straight (blue); Group C; twisted fibrils with bundled (green).

morphologies. Human a-syn formed twisted fibrils with wide (14.95 ± 2.09 nm) and narrow (8.51 ± 1.36 nm) components, and a periodicity of ∽110 nm (n = 10) (Fig. 1C). In contrast, the mouse a-syn fibrils showed straight types with its width (10.80 ± 1.04 nm) (n = 10) (Fig. 1D), and the cross-over points were difficult to identify in mouse straight-type fibrils. To examine the homogeneity of polymorphic fibrils, we counted the number of each fibril, and confirmed that human and mouse a-syn formed almost homogenous populations of distinct types of fibrils (100% and 97.52%), respectively. These results suggested that human and mouse a-syn formed prominently morphological distinct fibrils *in vitro*.

Partial digestion with various proteases has been used to reveal the biochemical property of different a-syn fibrils [19]. We performed the partial digestion with proteases to identify the difference between human and mouse a-syn fibrils. Proteinase K treatment differentiated human and mouse a-syn fibrils (human: slower digestion, mouse: rapid digestion), which is consistent with a previous report (Fig. 1E) [19]. Trypsin yielded additional differences between human a-syn and mouse a-syn fibrils (human: 2 bands, mouse: 3 bands at 20 s point) (Fig. S2B). These results suggested that human and mouse a-syn fibrils have different biochemical (protease digestion) properties.

In general, protein fibrillar aggregates are composed of a protease-resistant “core” and an associated “fuzzy coat”, which is susceptible to the proteolysis [26]. We tried to identify which region of an a-syn forms the protease-resistant core of the aggregates. A-syn aggregates were digested with a nonspecific protease, proteinase K to obtain proteinase K-resistant core of a-syn fibrils [27,28]. When we analyzed human a-syn amyloid core regions by MALDI-TOF mass spectrometry, we detected peaks at mainly m/z 9127.1, m/z 9539.4, m/z 10,914.7 in the spectra of digested human a-syn fibrils (the long cores) (Fig. 1G). In contrast, the peak for the protease-resistant fragment of mouse a-syn fibrils was mainly detected at m/z 7978.6 (the short core). These results revealed that the human and mouse a-syn fibrils contain different core regions and further supports the structural polymorphism of amyloid fibrils. Taken together, we conclude that human and mouse a-syn form two morphological and biochemical distinct amyloid fibrils.

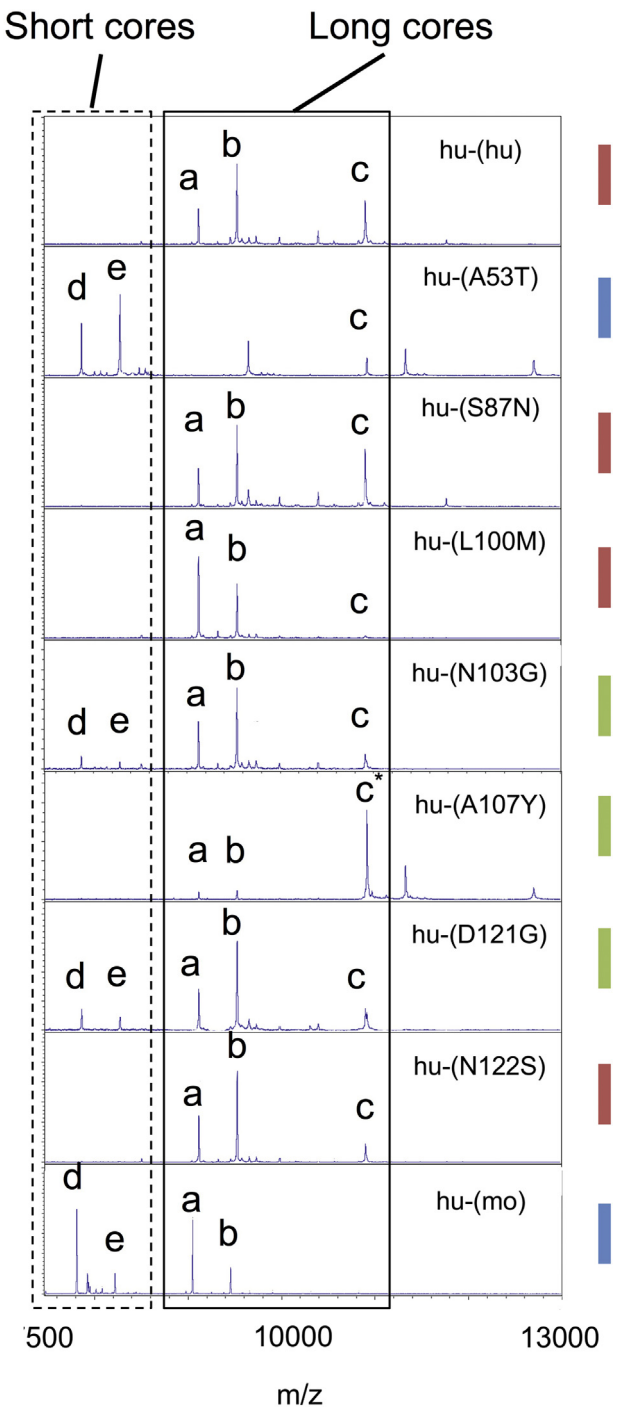

Fig. 6. Seed-induced aggregates showed distinct proteinase K-resistant cores corresponding to those of the pre-formed fibril used for seeds.
MALDI-TOF MS spectra (m/z 7500–13,000) of core peptides derived from seed induced aggregates of human WT a-syn with mutant PFF. Segments enclosed in rectangles with a solid and dashed lines are shown for long core (human-specific spectra area; a, b, c, c*) and short core (mouse-specific spectra area; d, e), respectively. There is minor difference in the spectra between c and c* in hu-(A107Y). The classification of morphologies; Group A (red), Group B (blue), and Group C (green) are indicated on the right side.

3.2. A53T substitution is a major determinant for the morphological and biochemical property of mouse a-syn fibril

To identify the amino acid(s) responsible for the structural differences between human and mouse a-syn fibrils, we generated the mutants of human a-syn containing each substitution of the different amino acid between human and mouse a-syn. We performed SDS-PAGE and Native-PAGE analysis for those mutants (Fig. S1). As shown in Fig. S1A, D121G migrated similar to mouse a-syn in Native-PAGE, clearly indicating that D121, with its negatively charged aspartate, is responsible for the electrophoretic mobility difference between human and mouse a-syn.

All seven point mutants of human a-syn formed amyloid fibrils *in vitro* under our experimental conditions (Fig. 2). Typically, human a-syn mutants substituted with S87N, L100M, and N122S (Group A) predominantly formed twisted types of fibrils (Fig. 2). In contrast, A53T formed straight types of fibrils (Group B) as observed in mouse a-syn. However, N103G, A107Y, and D121G showed both twisted and bundles (or pairs) of straight fibrils (Group C). The morphological analysis using EM suggests that a-syn fibrils show mutation-dependent structural polymorphism.

When comparing the partial digestion pattern of fibrils derived from those mutants by proteinase K, the digestion patterns did not correspond to the fibrillar morphology (Fig. S3A). N122S showed the digestion patterns, which is similar to mouse patterns, though predominant morphologies in N122S are twisted types. Additionally, the trypsin partial digestion pattern showed inconsistencies with the morphology, although 3 bands at 20 s of digestion bands of mouse a-syn were observed in A53T (Fig. S3B).

We further examined the protease resistant core of mutant a-syn fibrils using MALDI-TOF MS analysis. The protease resistant core also differed among a-syn mutant fibrils (Fig. 3). The long cores of human a-syn fibrils are designated as a (*m/z* 9127.1), b (*m/z* 9539.4), and c (*m/z* 10,914.7). The presence of a, b, and c signals in S87N, L100M, N103G, A107Y, D121G, and N122S were observed (Group A and Group C), though the rates of intensity were distinct. Despite the similar morphologies, N103G and A107Y showed distinct spectra in their rates of intensities. In contrast, the short core of mouse type (designated as d (*m/z* 7900.4), e (*m/z* 8312.7)) was observed in A53T in the spectra (Group B). A107Y and D121G also include the short core peak(s) though the intensities are relatively low. The minor differences in the peaks (a, b, c, d, and e) between human WT a-syn and mutants or between mouse a-syn and A53T were observed because the mass shifts were caused by amino acid substitutions.

Although the partial digestion patterns with proteases only partially correspond to the shape of amyloid fibrils, the protease-resistant cores are highly consistent with distinct morphologies of amyloid fibrils (twisted and twisted with bundles; long core, straight; short core). Thus, our results, for the first time, showed that the interspecies single substitutions used in our study can regulate distinct biochemical properties in different mutant a-syn aggregates. Additionally, focusing on the difference between human and mouse a-syn aggregates (Fig. 1), our results strongly suggested that a single substitution of A53T mainly regulated those morphological and biochemical differences.

Polymorphic aggregates derived from human and mouse a-syn could be classified as the biochemical and morphological properties. To examine the processes of aggregation, we used ThT fluorescence, which specifically binds to hydrogen bonds of the beta-sheet structure [30]. We assessed the aggregation kinetics of each mutant using ThT fluorescence at each time point (0 h, 4 h, 8 h, 24 h, and 168–192 h) (Fig. 4A). The nucleation phase of mouse a-syn was shorter than those of human a-syn and other mutants. Final ThT fluorescence intensity of A53T mutant is similar to that of mouse a-syn. Overall, no correlation of fibril structure of a-syn with nucleation phase nor aggregation rate except with final ThT intensity was observed (Fig. 4B).

3.3. Transmissibility of morphological and biochemical features by seeding

The results of the single substitutions experiments suggest the primary sequence of a-syn is a strong structural determinant for fibrils generated by spontaneous aggregation; however, it can be possible that

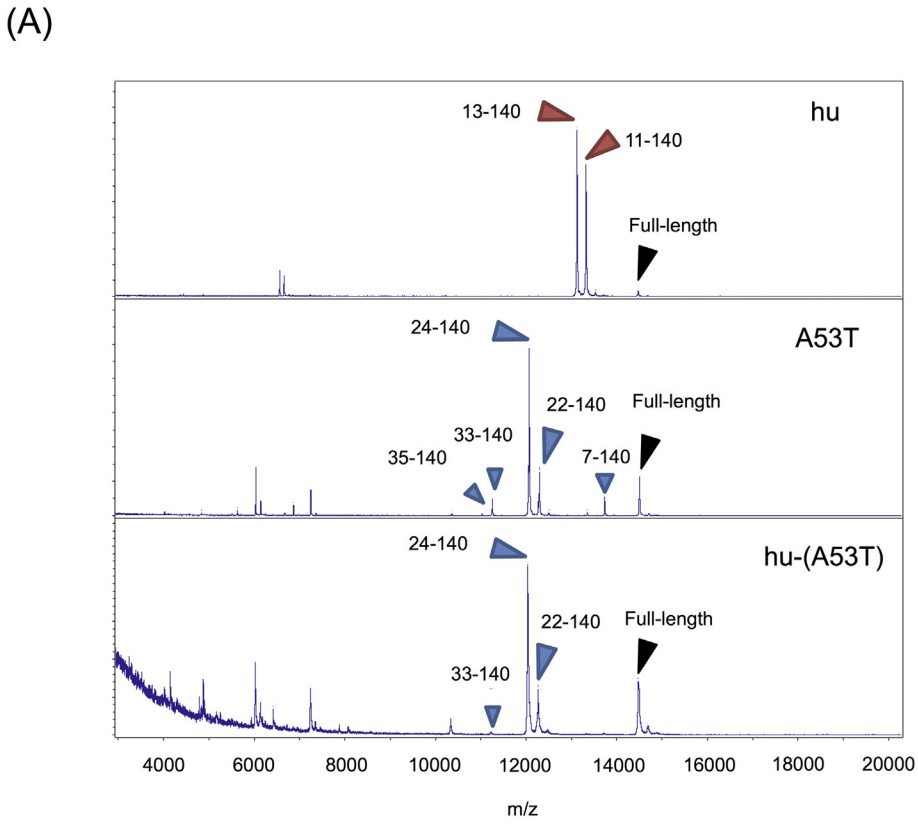

Fig. 7. Human, A53T, and human a-syn seeded with A53T (hu-(A53T)) fibrils showed distinct susceptibility against digestion by lysyl endopeptidase.
(A) The spectra of lysyl endopeptidase-resistant core. Obtained spectra were shown in Supplementary Tables 2–4. (B) Schematic representation of the lysyl endopeptidase cleavage sites of human a-syn. The color of the lysine residues in human a-syn is changed into red (K6, K10, K12, K21, K23, K32, K34, K43, K45, K58, K60, K80, K96, and K97). The cleavage sites are calculated using a software, FindPept. Red and blue arrowheads indicate human and A53T cleavage sites with lysyl endopeptidase, respectively. The size of arrowheads reflects the intensity of obtained mass spectra. The mutation site of A53 is underlined.

Table 1
Summary of the results in this study.

	Group A	Group B	Group C
Morphology	Twisted	Straight	Twisted with bundling
Protease-resistant core	Long core	Short core	Long core
Mutant	hu, S87N, L100M, N122S	A53T, mo	N103G, A107Y, D121G
Seed-induced structural transmission	N.D.	Yes	Yes

Note: N.D.: we could not determine the seed-induced structural transmission.

other factors regulate this process. In this respect, we performed seeding experiments to investigate whether seeds could induce structures different from the spontaneously-formed aggregates. We seeded human WT a-syn with the aggregates (PFF) of human, mouse or human point mutants (designated the pairs as hu-(seeds)). The predominant morphologies of hu-(hu), hu-(S87N), hu-(L100M), and hu-(N122S) aggregates are twisted-type of fibrils as observed in the PFF seeds (Group A) (Fig. 5). In contrast, the predominant morphology of hu-(A53T) and hu-(mo) are straight-type of fibrils as observed in those PFF seeds (Group B). Furthermore, hu-(N103G), hu-(A107Y), and hu-(D121G) showed both twisted and bundles of straight fibrils (Group C). Although the population was minor, we also observed twisted fibrils in all the seed-induced aggregates even in hu-(mo) and hu-(A53T), possibly because of spontaneous aggregation of human WT a-syn. These results indicate that the morphological structure of the PFF seeds could be transmitted to the substrate (human WT a-syn), generating the different structures from spontaneously formed aggregates of human WT a-syn.

We also examined the seeding efficiencies between human and mouse a-syn (Fig. 4B). As we expected, cross-seeding (hu-(mo)) resulted in a lower seeding efficiency than self-seeding (hu-(hu)), which was consistent with previous reports [16,19]. To examine the amino acid regulation of these interspecies seeding differences, we also performed the seeding experiments using the mutants with single substitutions.

Although all seeds shorten the delay of the initiation of the aggregation, the seeding efficiencies related to the propagation rate of aggregates in all mutant seeds were between that of human WT and mouse a-syn (Fig. 4C). When comparing the final ThT intensity in seed-induced aggregates, their values varied (Fig. 4D). Focusing on the morphological differences, these data indicated that the seeding efficiencies between human and mouse a-syn were irrespective of the morphologically difference.

To analyze the further biochemical properties of seed-induced aggregates, we performed protease digestion experiments using proteinase K as performed in Fig. S3. Upon protease partial digestion, the digestion patterns of mouse and N122S fibrils showed the different patterns from hu-(mo) and hu-(N122S) (Figs. S3A and S4A). However, other seed-induced aggregates showed band patterns nearly identical to those of the seeds. Thus, under these seeding conditions, human a-syn partly adopted the biochemical properties of the seeds, that was also shown in trypsin digestion patterns (Figs. S3B and S4B).

We further examined the amyloid fibrils cores of seed-induced aggregates (Fig. 6). Group A and C (hu-(hu), hu-(S87N), hu-(L100M), hu-(N103G), hu-(A107Y), hu-(D121G), and hu-(N122S)) showed human-type long core peaks (a, b, c). In contrast, protease-resistant core of Group B (hu-(A53T) and hu-(mo)) showed two major peaks, which corresponded to the mouse-type short core. Because spontaneous aggregation of human WT a-syn could occur under our experimental condition, seed-induced aggregates in Group B also included a and b or c peak(s) in addition to d and e peaks. These results suggest that the protease resistant core of human a-syn seeded with mutant aggregates included the core of the spontaneous aggregates of human a-syn. However, other mass peak(s) of hu-(A107Y) core (m/z 10,925.2, c*) did not correspond to those of human WT a-syn (m/z 10,914.7, c) and A107Y aggregates core (m/z 9217.3, a). At this moment, it is hard to explain this different peak pattern observed between PFF seeds and seed-induced aggregate of A107Y. One possibility is that A107Y PFF seeds include multiple conformational species and amplification of minor species, in which their cores are different from that of the seeds, occurred. Although minor differences were observed, the core patterns are highly consistent with those of the PFF seeds, strongly suggesting core structure transmission by seeding.

Because of low specificity of the digestion site by proteinase K, the protease-resistant core region is hardly identified. We used a sequence specific protease, lysyl endopeptidase to digest the obtained aggregates followed by MALDI-TOF-MS analysis (Fig. 7A and Tables S2–4). We found different peaks of the mass spectra between human and A53T mutants. The location of the peaks was clearly differed (human: 13125.8 and 13,325.9, A53T: 12069.5 and 12,299.0 (m/z)). We estimated the lysyl C-resistant cores by calculation from the mass spectra using a software, FindPept, indicating that the difference of two types of lysyl C-resistant cores were based on N-terminal regions of a-syn (human; 13,125.8: 13–140 and 13,325.946: 11–140, A53T; 12,069.4: 24–140 and 12,099.0: 22–140, (m/z): (amino acid)) (Fig. 7B). A53T lysyl C-resistant core was transmitted to human a-syn (hu-(A53T)) by seeding reaction (hu-(A53T): 12041.0 (m/z)). The minor differences in the peaks between A53T and hu-(A53T) were observed because the mass shifts were caused by amino acid substitutions. These data clearly suggested that human WT a-syn and A53T contain different protease-resistant core regions and could be cleaved at different N-terminal regions, and these structural features could be transmitted to human WT a-syn by seeding reaction.

4. Discussion

In this study, we found that spontaneous aggregation of human and mouse a-syn generated fibrils with distinct morphological and biochemical properties. In contrast, a-syn monomers were able to adopt the various structures upon seeding with different PFF seeds (Table 1). Particularly, a single interspecies substitution, A53T, one of the familial PD mutations, was responsible for formation of mouse-type structures including straight morphology and short protease-resistant core, which was completely transmitted to human a-syn by seeding. We thus identified novel structural properties of a-syn fibrils showing sequence- and seed-structure-dependent polymorphisms. Our results could be the structural basis for the polymorphic aggregates of a-syn involved in distinct pathogenicity of synucleinopathies [9,29].

Previous reports showed that human and mouse a-syn occasionally formed two types (straight and twisted) of fibrils [20,30], which might be due to subtle difference in fibrillization conditions [31]. In contrast, our present study showed the almost homogenous morphologies for human (twisted) and mouse (straight) a-syn fibrils (Fig. 1C and D, and Fig. S2). One possible reason for this discrepancy may be because the a-syn constructs used in this study are codon136 mutants (TAC to TAT), which avoid mis-incorporation of Cys at this position instead of original Tyr residue in *E. coli* [23]. Non-mutant a-syn, probably used in those previous studies, partially produces a-syn including C136, which could induce artificial a-syn dimerization to produce different types of fibrils. Alternatively, our a-syn constructs lack first Met but leave artificial N-terminal Gly-Ser residues after His-tag removal, which might affect some morphological organization of a-syn fibrils. Although we could not conclude why we could obtain homogenous morphology for human and mouse a-syn fibrils, using this construct, we could obtain the condition suitable for differentiating substitution effects between human and mouse a-syn.

Solid-state NMR revealed that human a-syn amyloid fibrils contain core residues (44–96) arranged in parallel β-sheets with a Greek-key topology [32]. Similar analysis using mouse a-syn indicate the presence of a structurally conserved motif comprising residues 61–80 [31]. In addition, recent research suggested that the mouse a-syn fibrils adopts a very similar core structure (residues 38–97) to that of human a-syn fibrils [21]. Recent Cryo-EM research demonstrated that human a-syn protofilaments were packed with two different regions, that is, NAC (residues 68–78) or pre-NAC (residues 46–56) regions, generating polymorphic a-syn fibrils with rod or twister structure, respectively [33]. Our identified twisted and straight types of fibrils mostly resemble these fibrillar polymorphs (twister and rod). These observations suggest that the protofilament core structure is conserved in mouse a-syn fibrils, but the interface for protofilament interaction may be different from that of human a-syn, resulting in generation of morphologically distinct straight fibrils. More precise structural analysis such as cryo-EM is, however, necessary.

We further found the difference in proteinase K-resistant core regions, longer in human twisted fibrils but shorter in mouse straight fibrils, which was highly corresponding to the morphological differences of the fibrils. Experiments using lysyl endopeptidase suggest that N-terminal 21–24 amino acid region is additionally resistant in human a-syn fibrils (Fig. 7). Previous research suggested possible roles of N-terminal region in determining the morphology of the fibrils [30,31,34]. Indeed, hydrogen–deuterium exchange mass spectrometry revealed that flat, ribbon-like fibrils had additional regions (residues 4–17 and 18–38) resistant for deuterium incorporation compraed with helical fibrils [34]. How N-terminal core is associated with the structural property is unclear. One possibility is the formation of an additional protofilament interface to alter the fibrillar morphology. Alternatively, it reflects the alteration of pre-existing interface because A53T substitution in mouse a-syn is located in the pre-NAC interface described above [33].

A series of experiments using human a-syn point mutants revealed that A53T was sufficient for structural conversion to straight fibrils. A53T substitution also shortened the N-terminal protease core region. A previous report described that PD-associated mutations such as A53T in human a-syn may affect pre-NAC-mediated protofilament interaction to alter the fibril morphology to twisted type [33]. However, our A53T mutant favored straight but not twisted morphology, implying A53T mutation could strengthen the protofilament interaction. In addition,

we recently found that most disease-associated mutants, including A30P, H50Q, G51D and A53E but not E46K, also favored straight fibrillar morphology [35]. Future cryo-EM analysis for these mutants may clarify this point.

In contrast to the previous reports describing that A53T substitution enhanced a-syn spontaneous aggregation [20], we observed decreased in aggregation rate of A53T as compared to human WT a-syn measured by ThT fluorescence (Fig. 4A). Although the reason of this partial discrepancy is uncertain, our data indicate the aggregation kinetics is not directly related to the structural properties.

In the experiments for short-term protease digestion, we found the high sensitivity of mouse a-syn fibrils against proteinase K, which was mimicked by N122S substitution (Fig. 1E and Fig. S3A). Interestingly, the N122S did not affect the protease-resistant core obtained by long-term incubation with proteinase K, and also did not alter the fibrillar morphology (Figs. 2 and 3). The short-term incubation may digest the surface amino acids composing fuzzy coat of amyloid fibrils [11]. We thus suggest that region around residue 122 composes the fuzzy coat and is not directly involved in the fibrillar morphogenesis. Again, A53T substitution slightly suppressed the digestion by short-term incubation but the band pattern was totally unaffected (Fig. S3A).

Finally, we observed transmission of the structural properties of straight fibrils after their seeding to human a-syn; this phenomenon was more prominent for A53T fibrils. Because A53T is one of disease-associated mutations, the structural transmission suggests the propagation of potentially pathogenic conformer once the fibrils were formed. The A53T mutation may alter property of the interphase for protofilament interactions, leading to alteration of fibrillar morphology. In addition to A53T, we recently reported that disease-related other mutants including A30P, H50Q, G51D and A53E also formed straight types of fibrils containing different protease-resistant cores [35]. Further studies focused on disease-associated mutants and their structural propagation may deepen our understanding of how a-syn structural polymorphism mediates distinct pathogenicity of synucleinopathies.

Author contributions

G.T. mainly performed the experiments, N. Kajimura and K. Mitsuoka supported EM analysis, G.T., T.Y., Y.F, and N.N. designed the experiments and wrote the manuscript.

Transparency document

The Transparency document associated with this article can be found, in online version.

Acknowledgments

The authors thank Edward William Ko Uy for English editing of the manuscript, and Sakiko Fujita (NAIST, Nara, Japan) for technical support. We thank the Support Unit for Bio-Material Analysis, RIKEN BSI Research Resources Center, especially Aya Abe and Kaori Otsuki for mass spectrometric analysis. We also thank the Doshisha University Faculty of Life and Medical Sciences, especially Junko Naritomi, for DNA sequencing. This work was supported by Japan Agency for Medical Research and Development, AMED under Grant Number JP18dm0107140 to N.N and from the Ministry of Education, Culture, Sports, Science and Technology (MEXT) of Japan to N.N. (17H01564), to T.Y. (15K06762, 17KT0131) and to G.T. (17J05799). A part of this work was supported by Advanced Characterization Nanotechnology Platform, Nanotechnology Platform Program of MEXT, Japan at the Research Center for Ultra-High Voltage Electron Microscopy (Nanotechnology Open Facilities) in Osaka University. A part of this work was conducted in NAIST, supported by Nanotechnology Platform Program (Synthesis of Molecules and Materials) of the MEXT.

Appendix A. Supplementary data

Supplementary data to this article can be found online at https://doi.org/10.1016/j.bbadis.2019.02.013.

References

[1] C.A. Ross, M.A. Poirier, Protein aggregation and neurodegenerative disease, Nat. Med. 10 (Suppl) (2004) S10–S17.
[2] K.A. Jellinger, Neuropathological spectrum of synucleinopathies, Mov. Disord. 18 (Suppl. 6) (2003) S2–12.
[3] M.G. Spillantini, R.A. Crowther, R. Jakes, M. Hasegawa, M. Goedert, alpha-Synuclein in filamentous inclusions of Lewy bodies from Parkinson's disease and dementia with lewy bodies, Proc. Natl. Acad. Sci. U. S. A. 95 (1998) 6469–6473.
[4] K. Wakabayashi, M. Yoshimoto, S. Tsuji, H. Takahashi, Alpha-synuclein immunoreactivity in glial cytoplasmic inclusions in multiple system atrophy, Neurosci. Lett. 249 (1998) 180–182.
[5] J.C. Watts, K. Giles, A. Oehler, L. Middleton, D.T. Dexter, S.M. Gentleman, S.J. DeArmond, S.B. Prusiner, Transmission of multiple system atrophy prions to transgenic mice, Proc. Natl. Acad. Sci. U. S. A. 110 (2013) 19555–19560.
[6] A.L. Woerman, J. Stohr, A. Aoyagi, R. Rampersaud, Z. Krejciova, J.C. Watts, T. Ohyama, S. Patel, K. Widjaja, A. Oehler, D.W. Sanders, M.I. Diamond, W.W. Seeley, L.T. Middleton, S.M. Gentleman, D.A. Mordes, T.C. Sudhof, K. Giles, S.B. Prusiner, Propagation of prions causing synucleinopathies in cultured cells, Proc. Natl. Acad. Sci. U. S. A. 112 (2015) E4949–E4958.
[7] S.B. Prusiner, A.L. Woerman, D.A. Mordes, J.C. Watts, R. Rampersaud, D.B. Berry, S. Patel, A. Oehler, J.K. Lowe, S.N. Kravitz, D.H. Geschwind, D.V. Glidden, G.M. Halliday, L.T. Middleton, S.M. Gentleman, L.T. Grinberg, K. Giles, Evidence for alpha-synuclein prions causing multiple system atrophy in humans with parkinsonism, Proc. Natl. Acad. Sci. U. S. A. 112 (2015) E5308–E5317.
[8] A.L. Woerman, S.A. Kazmi, S. Patel, Y. Freyman, A. Oehler, A. Aoyagi, D.A. Mordes, G.M. Halliday, L.T. Middleton, S.M. Gentleman, S.H. Olson, S.B. Prusiner, MSA prions exhibit remarkable stability and resistance to inactivation, Acta Neuropathol. 135 (2018) 49–63.
[9] C. Peng, R.J. Gathagan, D.J. Covell, C. Medellin, A. Stieber, J.L. Robinson, B. Zhang, R.M. Pitkin, M.F. Olufemi, K.C. Luk, J.Q. Trojanowski, V.M. Lee, Cellular milieu imparts distinct pathological alpha-synuclein strains in alpha-synucleinopathies, Nature 557 (2018) 558–563.
[10] W. Peelaerts, L. Bousset, A. Van der Perren, A. Moskalyuk, R. Pulizzi, M. Giugliano, C. Van den Haute, R. Melki, V. Baekelandt, alpha-Synuclein strains cause distinct synucleinopathies after local and systemic administration, Nature 522 (2015) 340–344.
[11] J.L. Guo, D.J. Covell, J.P. Daniels, M. Iba, A. Stieber, B. Zhang, D.M. Riddle, L.K. Kwong, Y. Xu, J.Q. Trojanowski, V.M. Lee, Distinct alpha-synuclein strains differentially promote tau inclusions in neurons, Cell 154 (2013) 103–117.
[12] C. Kim, G. Lv, J.S. Lee, B.C. Jung, M. Masuda-Suzukake, C.S. Hong, E. Valera, H.J. Lee, S.R. Paik, M. Hasegawa, E. Masliah, D. Eliezer, S.J. Lee, Exposure to bacterial endotoxin generates a distinct strain of alpha-synuclein fibril, Sci. Rep. 6 (2016) 30891.
[13] P. Chien, J.S. Weissman, Conformational diversity in a yeast prion dictates its seeding specificity, Nature 410 (2001) 223–227.
[14] R.A. Moore, I. Vorberg, S.A. Priola, Species barriers in prion diseases—brief review, Arch. Virol. Suppl. (2005) 187–202.
[15] D.A. Kocisko, S.A. Priola, G.J. Raymond, B. Chesebro, P.T. Lansbury Jr., B. Caughey, Species specificity in the cell-free conversion of prion protein to protease-resistant forms: a model for the scrapie species barrier, Proc. Natl. Acad. Sci. U. S. A. 92 (1995) 3923–3927.
[16] M.B. Fares, B. Maco, A. Oueslati, E. Rockenstein, N. Ninkina, V.L. Buchman, E. Masliah, H.A. Lashuel, Induction of de novo alpha-synuclein fibrillization in a neuronal model for Parkinson's disease, Proc. Natl. Acad. Sci. U. S. A. 113 (2016) E912–E921.
[17] M. Masuda-Suzukake, T. Nonaka, M. Hosokawa, T. Oikawa, T. Arai, H. Akiyama, D.M. Mann, M. Hasegawa, Prion-like spreading of pathological alpha-synuclein in brain, Brain 136 (2013) 1128–1138.
[18] A. Okuzumi, M. Kurosawa, T. Hatano, M. Takanashi, S. Nojiri, T. Fukuhara, T. Yamanaka, H. Miyazaki, S. Yoshinaga, Y. Furukawa, T. Shimogori, N. Hattori, N. Nukina, Rapid dissemination of alpha-synuclein seeds through neural circuits in an in-vivo prion-like seeding experiment, Acta Neuropathol. Commun. 6 (2018) 96.
[19] K.C. Luk, D.J. Covell, V.M. Kehm, B. Zhang, I.Y. Song, M.D. Byrne, R.M. Pitkin, S.C. Decker, J.Q. Trojanowski, V.M. Lee, Molecular and biological compatibility with host alpha-synuclein influences fibril pathogenicity, Cell Rep. 16 (2016) 3373–3387.
[20] L. Kang, K.P. Wu, M. Vendruscolo, J. Baum, The A53T mutation is key in defining the differences in the aggregation kinetics of human and mouse alpha-synuclein, J. Am. Chem. Soc. 133 (2011) 13465–13470.
[21] G. Lv, A. Kumar, Y. Huang, D. Eliezer, A protofilament-protofilament interface in the structure of mouse alpha-synuclein fibrils, Biophys. J. 114 (2018) 2811–2819.
[22] S. Hwang, P. Fricke, M. Zinke, K. Giller, J.S. Wall, D. Riedel, S. Becker, A. Lange, Comparison of the 3D structures of mouse and human alpha-synuclein fibrils by solid-state NMR and STEM, J. Struct. Biol. (2018), https://doi.org/10.1016/j.jsb.2018.04.003 pii: S1047-8477(18)30093-5. [Epub ahead of print].
[23] M. Masuda, N. Dohmae, T. Nonaka, T. Oikawa, S. Hisanaga, M. Goedert, M. Hasegawa, Cysteine misincorporation in bacterially expressed human alpha-synuclein, FEBS Lett. 580 (2006) 1775–1779.

[24] L. Bousset, L. Pieri, G. Ruiz-Arlandis, J. Gath, P.H. Jensen, B. Habenstein, K. Madiona, V. Olieric, A. Bockmann, B.H. Meier, R. Melki, Structural and functional characterization of two alpha-synuclein strains, Nat. Commun. 4 (2013) 2575.
[25] Y. Ohhashi, Y. Yamaguchi, H. Kurahashi, Y.O. Kamatari, S. Sugiyama, B. Uluca, T. Piechatzek, Y. Komi, T. Shida, H. Muller, S. Hanashima, H. Heise, K. Kuwata, M. Tanaka, Molecular basis for diversification of yeast prion strain conformation, Proc. Natl. Acad. Sci. U. S. A. 115 (2018) 2389–2394.
[26] C.M. Wischik, M. Novak, H.C. Thogersen, P.C. Edwards, M.J. Runswick, R. Jakes, J.E. Walker, C. Milstein, M. Roth, A. Klug, Isolation of a fragment of tau derived from the core of the paired helical filament of Alzheimer disease, Proc. Natl. Acad. Sci. U. S. A. 85 (1988) 4506–4510.
[27] Y. Furukawa, K. Kaneko, N. Nukina, Tau protein assembles into isoform- and disulfide-dependent polymorphic fibrils with distinct structural properties, J. Biol. Chem. 286 (2011) 27236–27246.
[28] Y. Furukawa, K. Kaneko, K. Yamanaka, N. Nukina, Mutation-dependent polymorphism of Cu,Zn-superoxide dismutase aggregates in the familial form of amyotrophic lateral sclerosis, J. Biol. Chem. 285 (2010) 22221–22231.
[29] R. Melki, Role of different alpha-synuclein strains in synucleinopathies, similarities with other neurodegenerative diseases, J. Park. Dis. 5 (2015) 217–227.
[30] H. Heise, W. Hoyer, S. Becker, O.C. Andronesi, D. Riedel, M. Baldus, Molecular-level secondary structure, polymorphism, and dynamics of full-length alpha-synuclein fibrils studied by solid-state NMR, Proc. Natl. Acad. Sci. U. S. A. 102 (2005) 15871–15876.
[31] G. Lv, A. Kumar, K. Giller, M.L. Orcellet, D. Riedel, C.O. Fernandez, S. Becker, A. Lange, Structural comparison of mouse and human alpha-synuclein amyloid fibrils by solid-state NMR, J. Mol. Biol. 420 (2012) 99–111.
[32] M.D. Tuttle, G. Comellas, A.J. Nieuwkoop, D.J. Covell, D.A. Berthold, K.D. Kloepper, J.M. Courtney, J.K. Kim, A.M. Barclay, A. Kendall, W. Wan, G. Stubbs, C.D. Schwieters, V.M. Lee, J.M. George, C.M. Rienstra, Solid-state NMR structure of a pathogenic fibril of full-length human alpha-synuclein, Nat. Struct. Mol. Biol. 23 (2016) 409–415.
[33] B. Li, P. Ge, K.A. Murray, P. Sheth, M. Zhang, G. Nair, M.R. Sawaya, W.S. Shin, D.R. Boyer, S. Ye, D.S. Eisenberg, Z.H. Zhou, L. Jiang, Cryo-EM of full-length alpha-synuclein reveals fibril polymorphs with a common structural kernel, Nat. Commun. 9 (2018) 3609.
[34] H. Kumar, J. Singh, P. Kumari, J.B. Udgaonkar, Modulation of the extent of structural heterogeneity in alpha-synuclein fibrils by the small molecule thioflavin T, J. Biol. Chem. 292 (2017) 16891–16903.
[35] G. Tanaka, T. Yamanaka, Y. Furukawa, N. Kajimura, K. Mitsuoka, N. Nukina, Biochemical and morphological classification of disease-associated alpha-synuclein mutants aggregates, Biochem. Biophys. Res. Commun. 508 (3) (2019) 729–734.